nature nanotechnology

Article

https://doi.org/10.1038/s41565-024-01612-6

A non-FRET DNA reporter that changes fluorescence colour upon nuclease digestion

Received: 9 June 2023

Accepted: 15 January 2024

Published online: 13 February 2024



Check for updates

Soonwoo Hong 1, Jada N. Walker 2, Aaron T. Luong, Jonathan Mathews 1, Samuel W. J. Shields², Yu-An Kuo¹, Yuan-I Chen¹, Trung Duc Nguyen¹, Yujie He 1, Yu Anh-Thu Nguyen¹, Madhav L. Ghimire ® ³, Min Jun Kim ® ³, Jennifer S. Brodbelt² & Hsin-Chih Yeh 10 1,4

Fluorescence resonance energy transfer (FRET) reporters are commonly used in the final stages of nucleic acid amplification tests to indicate the presence of nucleic acid targets, where fluorescence is restored by nucleases that cleave the FRET reporters. However, the need for dual labelling and purification during manufacturing contributes to the high cost of FRET reporters. Here we demonstrate a low-cost silver nanocluster reporter that does not rely on FRET as the on/off switching mechanism, but rather on a cluster transformation process that leads to fluorescence color change upon nuclease digestion. Notably, a 90 nm red shift in emission is observed upon reporter cleavage, a result unattainable by a simple donor-quencher FRET reporter. Electrospray ionization-mass spectrometry results suggest that the stoichiometric change of the silver nanoclusters from Ag₁₃ (in the intact DNA host) to Ag_{10} (in the fragments) is probably responsible for the emission colour change observed after reporter digestion. Our results demonstrate that DNA-templated silver nanocluster probes can be versatile reporters for detecting nuclease activities and provide insights into the interactions between nucleases and metallo-DNA nanomaterials.

While recent advances in nucleic acid detection methods have bypassed the need for specialized equipment¹⁻³, the highly reliable and sensitive nucleic acid assays still rely on fluorescence detection in their final stages^{4,5}. For instance, TaqMan⁶ and DNaseAlert⁴ are the most commonly used fluorescent reporters in quantitative PCR and DNA endonuclease-targeted clustered regularly interspaced short palindromic repeats (CRISPR) trans reporter (DETECTR)^{4,7} assays, respectively. Although these fluorescence resonance energy transfer (FRET) reporters light up upon digestion by Taq polymerase or Cas12a, with the restored fluorescence reflecting the abundance of the target^{4,7}, they are merely turn-on sensors that only rely on emission intensity for quantification. Notably, a no-target control is always required to provide a baseline for intensity comparison⁴, given that undigested FRET reporters are not completely dark⁸. Furthermore, FRET reporters require dual labelling of the oligonucleotides with a donor and a quencher at each end, and the need to remove excess reactants and singly labelled impurities during manufacturing contributes to the increased probe cost⁹. Thus, there is an unmet need to develop a low-cost substitute that does not rely on FRET for signal transduction and can provide a more quantitative sensing result upon nuclease digestion (for example, changing emission colour rather than changing intensity).

Department of Biomedical Engineering, The University of Texas at Austin, Austin, TX, USA. Department of Chemistry, The University of Texas at Austin, Austin, TX, USA. 3Department of Mechanical Engineering, Southern Methodist University, Dallas, TX, USA. 4Texas Materials Institute, The University of Texas at Austin, Austin, TX, USA.

☐e-mail: tim.yeh@austin.utexas.edu

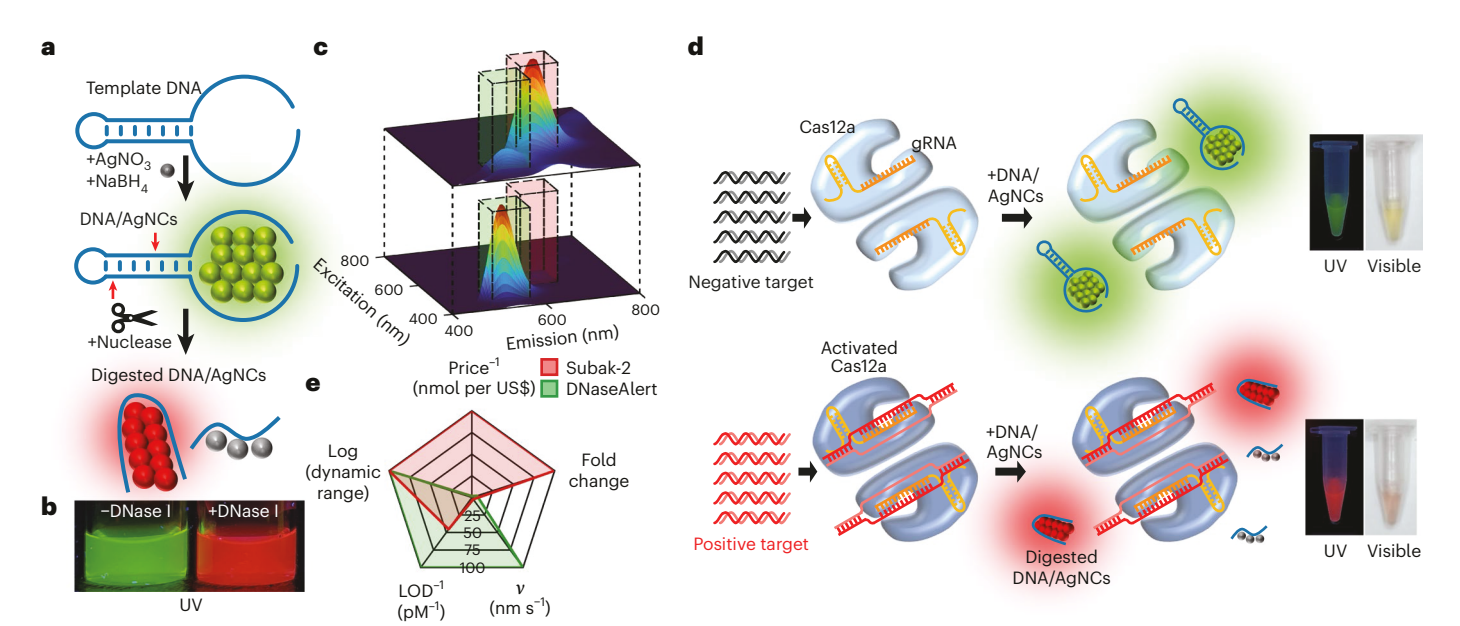


Fig. 1| A schematic of Subak reporters and their fragmentation-induced colour-switching property. a, Subak reporters are fluorescent silver nanoclusters hosted in hairpin DNA strands that change emission colour upon nuclease digestion. b, Photograph images under UV excitation (365 nm). DNA/AgNCs can be universally excited by a UV light source. Upon adding 5 μ g μ l⁻¹ DNase I to a purified 20 μ M Subak-1 solution, an obvious change in emission colour (from green to red) is seen within 20 min. c, Three-dimensional fluorescence spectra before (bottom) and after (top) DNase I digestion. In Subak-1, the green emitters (excitation/emission: 480/540 nm) are directly converted into the red emitters (excitation/emission: 565/630 nm) upon DNase I fragmentation, showing a red shift of 90 nm in the emission spectrum.

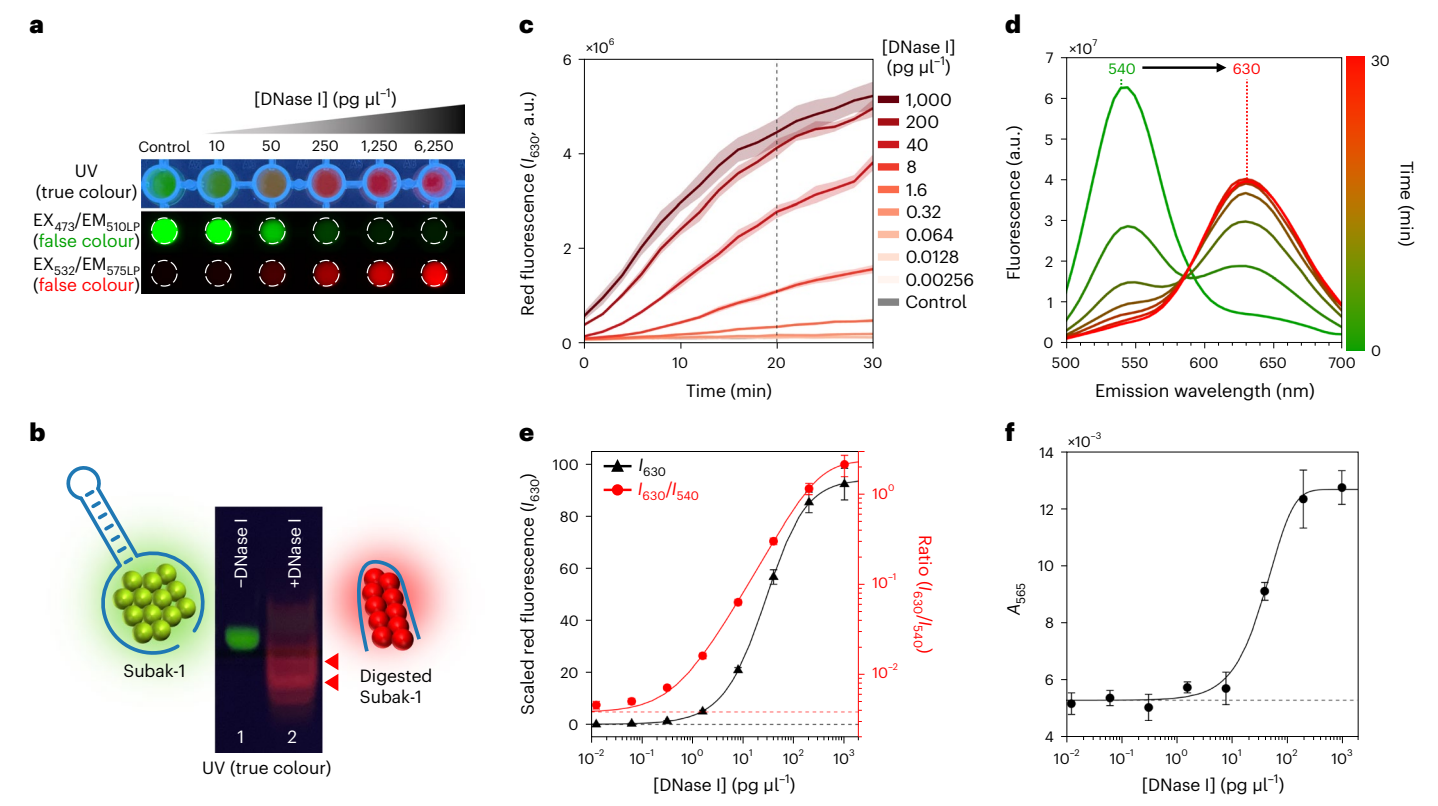
The green and red boxes represent the bandwidths (40 nm) of the excitation/emission filter pairs in the green and red detection channels, respectively. The fluorescence enhancement ratio of Subak-1 upon digestion is as high as 20-fold. ${\bf d}$, In a DETECTR assay, in the presence of target strands, Cas12a unleashes its trans cleavage activity, which fragments Subak-2 and changes its colour. Subak reporters are not only fluorescence sensors but also colorimetric sensors. In Subak-2, a change of absorption peak from 480 nm to 560 nm is observed after Cas12a cleavage. ${\bf e}$, A radar chart comparison between Subak and DNaseAlert. Compared with DNaseAlert, Subak-2 has one-sixtieth of the cost and offers 15 times higher fold change with comparable LOD (-1.19 pM) and dynamic range but the reaction velocity (ν) is 36 times slower.

In this Article, we describe a DNA-templated silver nanocluster (DNA/AgNC) probe termed Subak (which means 'watermelon' in Korean, Fig. 1a) for nuclease activity detection. Subak exhibits a green fluorescence emission (540 nm) in its intact form but changes its emission colour to bright red (630 nm) when fragmented due to nuclease activities. This fragmentation-induced colour-switching property is not known to be shared among other highly fluorescent nanomaterial probes. Compared with the commercially available FRET reporters, Subak has a substantially lower cost (US\$1 versus US\$62 per nanomole) and supports ratiometric sensing of nuclease activities as well as single-colour detection. As all DNA/AgNCs can be effectively excited by a ultraviolet (UV) light source 10-12, the fluorescence colour change of Subak after fragmentation can be easily seen by the naked eye under a UV lamp (Fig. 1b), even for the unpurified Subak (Supplementary Fig. 1).

The colour-switching mechanism behind Subak is not FRET, but rather a combinatorial effect of the altered base-cluster interacting footprint and the changed size/shape of the fragmented silver nanocluster (AgNC). Using electrospray ionization-mass spectrometry (ESI-MS)¹³, we have identified the preferred cleavage sites of the Subak reporters and the silver stoichiometries (the total number of silvers, $N_0 + N_{Ag+r}$ in a cluster) before and after fragmentation. We speculate that the green emission of intact Subak (Subak-1) originates from Ag_{13} and Ag₁₄ clusters, while the red emission of the fragmented Subak comes from a Ag_{10} cluster. The breakdown of Ag_{13} into Ag_{10} and Ag_3 underlies the fragmentation-induced colour-switching property of Subak reporters. Unlike the traditional nucleation-and-reduction methods that typically produce Ag₁₀ clusters with low or green fluorescence emission^{13–15}, post-processing methods such as complementary strand hybridization 9,16,17 and DNA host fragmentation (this report) could generate bright red-emitting Ag₁₀. We believe these post-processing steps not only change the AgNC stoichiometry (for example, an additive process from -Ag₁ to -Ag₁₁ during strand hybridization or a subtractive process from Ag₁₃ to Ag₁₀ during strand fragmentation in this report), but transform the AgNC into a new geometry with a footprint in the DNA host that is unattainable by the traditional nucleation-and-reduction method (Supplementary Fig. 2). This combinatorial effect results in the colour-switching phenomenon observed in Subak. Although some AgNC probes were previously reported to detect nuclease activities, they are turn-off sensors or require multiple steps in detection hortzet for detecting nuclease activities in nucleic acid detection assays. The fragmentation method outlined here also provides a strategy to create new types of AgNC fluorophores that were previously unattainable by the traditional nucleation-and-reduction process.

Subak design and nuclease activity detection

Subak reporters were prepared in hairpin DNA templates using the conventional nucleation-and-reduction process to form AgNCs in DNA 20,21 (Fig. 1a and Methods). We started our investigation among short strands (for example, 10 nt oligomers) as the biophysical properties of their hosted AgNCs were well characterized 14,22 . Despite the potential for these DNA/AgNC probes to exhibit strong fluorescence, they did not display any discernible colour change upon fragmentation (Supplementary Fig. 3a). This could be attributed to the fact that most bases in short strands directly interact with the encapsulated AgNCs 23 , making the strands resistant to nuclease cleavage. When moving from short strands to longer strands (>30 nt), we eventually found a 34 nt hairpin structure that gives a small but reliable emission peak red shift upon DNase I digestion (from 570 to 580 nm, Supplementary Fig. 3b–d). This hairpin construct served as a starting point for Subak evolution (Supplementary Table 1 and Supplementary Fig. 4). Although



 $\label{eq:Fig.2} \textbf{Quantification of DNase I using Subak-1. a}, \textbf{Subak-1} in a 96-well plate under UV excitation (top) and the corresponding laser-scanned images under 473 nm and 532 nm laser excitation (EX) (bottom). Laser-scanned images were false coloured in green (510 nm long-pass (LP) emission (EM) filter used) and red (575 nm LP EM filter used) on the basis of fluorescence intensity, respectively. DNase I concentration increased from 0 to 6,250 pg <math>\mu$ l⁻¹ (from left to right). **b**, Twenty per cent PAGE showed the true fluorescence colour of Subak-1 before and after DNase I digestion under UV excitation. The intact green Subak-1 reporters were cleaved into red fragments, where two major red-fragment species were noted (red triangles). **c**, Fluorescence emission spectra of Subak-1 in response to various amounts of DNase I. The red fluorescence (I_{630}) was measured at 630 nm under 565 nm

excitation. The lines represent the mean values, while the shadings represent the standard deviations (n=3 replicates). **d**, Time-dependent fluorescence spectra were measured every 5 min under 280 nm excitation. **e**, Single-colour (I_{630}) and ratiometric sensing (I_{630}/I_{540}) results of purified Subak-1 on DNase I. The green fluorescence (I_{540}) was measured at 540 nm under 480 nm excitation, while the red fluorescence (I_{630}) was measured at 630 nm under 565 nm excitation. **f**, Absorption at 565 nm (I_{630}) was measured using a plate reader. Both fluorescence and absorption were measured after 20 min of incubation at 37 °C. Sigmoidal regression curves were fitted using a weighted 5-PL regression (Supplementary Equation 2). The error bars represent the standard deviations (I_{60}) are plicates), while dashed lines represent the mean background values from the blank samples.

the fragmentation-induced colour-switching property of Subak was first evaluated using DNase I as a model enzyme (Fig. 1b,c), our main goal was to develop AgNC probes that can respond to nucleases used in the nucleic acid detection assays (such as Cas12a in the DETECTR assay, Fig. 1d).

Subak reporter design consisted of three parts—a loop, a stem and two overhang arms (5′-arm and 3′-arm). The loop was composed of only thymines, which have minimum interactions with the encapsulated AgNC²⁴. The stem was 7-bp-long, which holds the preferred nuclease cleavage sites. The overhangs (5′-arm and 3′-arm) were designed based on the previous reports in fabricating highly emissive DNA/AgNC probes (Supplementary Fig. 5)^{20,22}. Two Subak reporters, Subak-1 and Subak-2, were our primary interest for investigation, where Subak-1 was specifically designed for DNase I activity detection (Fig. 1a–c) while Subak-2 was tailored for Cas12a *trans* cleavage in the DETECTR assay (Fig. 1d,e).

Subak-1 suspended in the DNase reaction buffer was mixed with different concentrations of DNase I (from 0 to 6,250 pg µl⁻¹) to quantify the nuclease activity (Fig. 2). The buffer only induced a minor emission red shift in Subak-1 (from 530 nm to 540 nm, Supplementary Fig. 6). Upon addition of DNase I, the colour of the Subak-1 solution gradually changed from green (peak at 540 nm) to red (peak at 630 nm) in 20 min (Fig. 2a). Polyacrylamide gel electrophoresis (PAGE) further confirmed the fragmented Subak-1 to be red (Fig. 2b). The green and red gel bands shown in the figure were the true colours of intact and

fragmented Subak-1 reporters under UV excitation, respectively. Although unpurified Subak worked well in detection (Supplementary Fig. 1), gel-purified Subak was employed for more precise quantification of nuclease activities throughout this investigation (Fig. 2b and Supplementary Fig. 7).

The fluorescence conversion (from green, I_{540} , to red, I_{630}) correlated well with the DNase I quantity (Fig. 2c), with a clear isoemissive point in the emission spectrum (Fig. 2d and Supplementary Videos I and 2). Using these two distinct emission peaks (I_{540} and I_{630}), highly quantitative and reproducible ratiometric sensing of nuclease activity was obtained (I_{630}/I_{540} , Fig. 2e), which outperformed the red fluorescence-only quantification (I_{630} , Fig. 2e) in both the dynamic range (10^4 versus 10^2) and limit of detection (LOD, 3 versus 53 fg μ l⁻¹). Subak also supported colorimetric sensing. The increase in absorbance at 565 nm (I_{565}) correlated well with increasing DNase I concentration (Fig. 2f, Supplementary Fig. 8 and Supplementary Videos 3 and 4).

In the gel image, two fragment bands in lane 2 were particularly noted (red triangles in Fig. 2b) whereas the cleavage patterns of the DNA-only sample were more diverse (Supplementary Fig. 9), suggesting the presence of preferred cleavage sites in Subak-1. Earlier findings indicated that the footprint sizes of two spectrally distinct Ag_{10} chromophores may substantially vary within their respective DNA hosts¹³. It is possible that AgNC serves as a nuclease cleavage mask and its footprint determines the preferred cleavage sites in DNA.

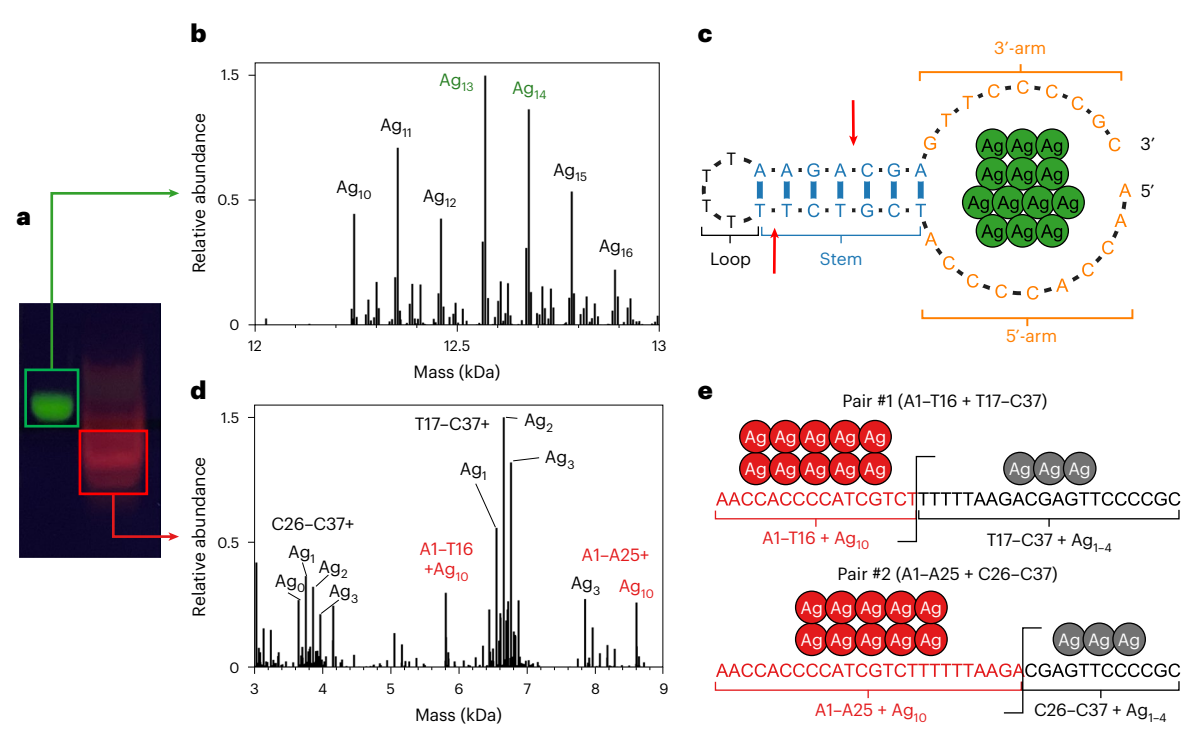


Fig. 3 | ESI–MS results of the gel-purified Subak-1 reporters before and after DNase I digestion. a, Gel-purified Subak-1 reporters before (green) and after digestion (red) were characterized by ESI–MS. b, Deconvoluted MS1 spectrum of Subak-1 before digestion. The dominant species of the freshly prepared, gel-purified sample contained Ag $_{13}$ and Ag $_{14}$. c, Hypothetical configuration of Ag $_{13}$ cluster in Subak-1. It is possible that three silver atoms in Ag $_{13}$ are on the outer face of the cluster, which are weakly associated with the rest of the silver atoms

that are strongly templated in the 5'-arm. ${\bf d}$, Deconvoluted MS1 spectrum of the digested Subak-1. Ag $_{13}$ or Ag $_{14}$ clusters in the intact Subak-1 template decomposed into Ag $_{10}$ and Ag $_{1-4}$ in the two 5'-arm fragments (A1–T16 and A1–A25) and the two 3'-arm fragments (T17–C37 and C26–C37), respectively. ${\bf e}$, We hypothesize that Ag $_{10}$ clusters in the two 5'-arm fragments (A1–T16 and A1–A25) are responsible for the observed red fluorescence, while Ag $_{1-4}$ in the two 3'-arm fragments are non-emissive.

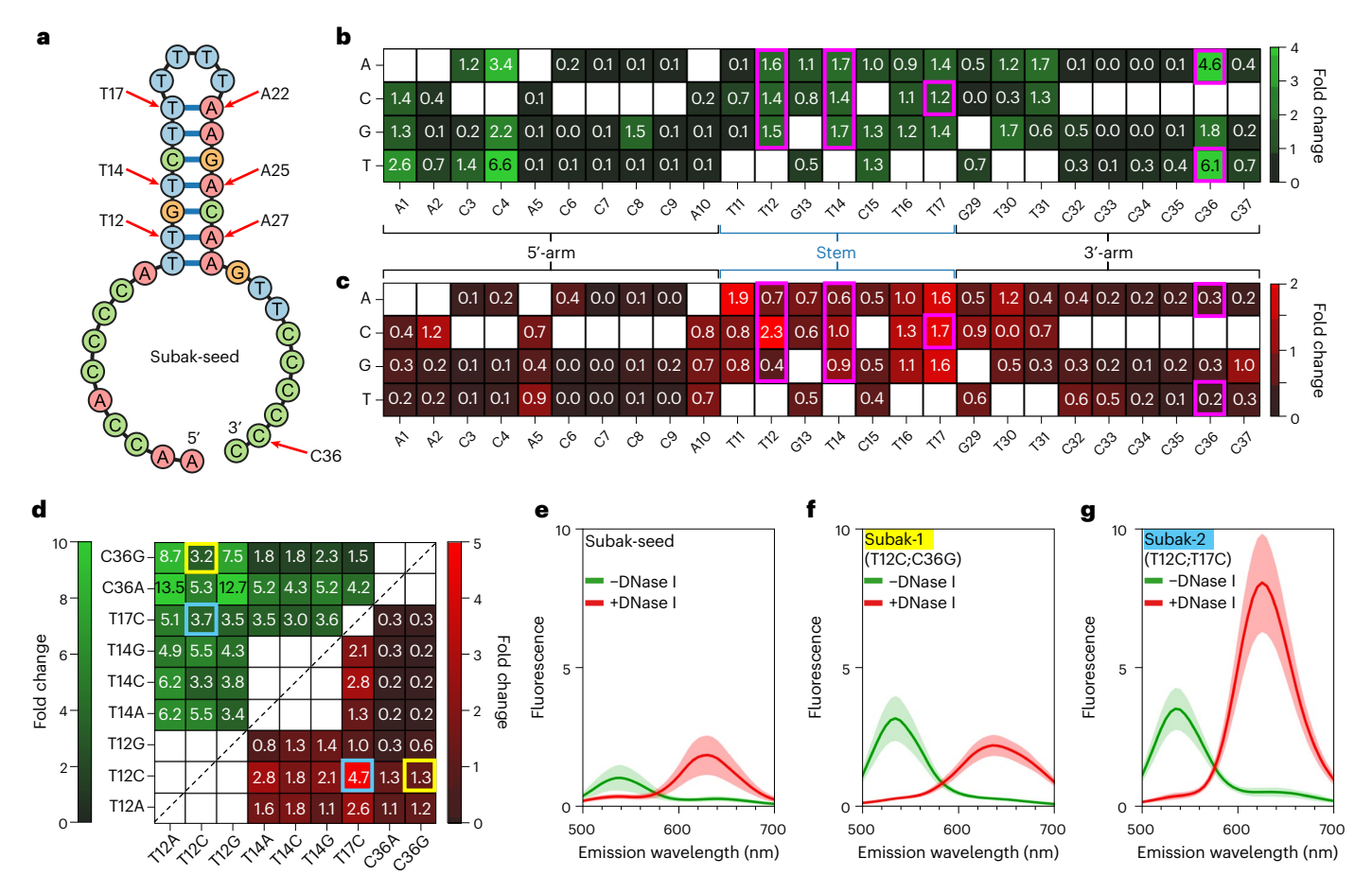
MS characterization

The gel-purified Subak-1 samples were further analysed by ESI-MS to identify their silver stoichiometries (Fig. 3a)13,20. The ESI-MS results indicated that the dominant species in intact Subak-1 are Ag₁₃ and Ag₁₄ (Fig. 3b,c). While other minor species (Ag $_{10}$, Ag $_{11}$, Ag $_{12}$, Ag $_{15}$ and Ag $_{16}$ in Fig. 3b) might also exhibit green emission, Ag₁₃ and Ag₁₄ were believed to be the main contributors to the observed green fluorescence. This prominence was attributed to the gel-purification process, which effectively preserved Ag₁₃/Ag₁₄ species and the green emission, while suppressing all other species (Supplementary Fig. 7). To completely remove the minor species from the sample, a different purification scheme, such as high-performance liquid chromatography¹⁶, is needed. Using isotope pattern analysis 16,25 , we further confirmed that the Ag₁₃ is actually a Ag₁₃⁹⁺ cluster while the Ag₁₄ is a Ag₁₄⁹⁺ cluster (Supplementary Figs. 10-12). With four and five neutral Ag atoms in their respective cores, Ag_{13}^{9+} and Ag_{14}^{9+} could be green chromophores with distinct chemical stability ^{16,26}. Indeed, we observed that Ag_{13}^{9+} (with an even number of valence electrons) is more stable than Ag₁₄ ⁹⁺ (with an odd number of valence electrons) over 4 weeks (Supplementary Fig. 13).

The two preferred cleavage sites in Subak-1 by DNase I were found in between T16/T17 and A25/C26 within the stem (red arrows in Fig. 3c), generating two 5'-arm fragments (A1–T16 and A1–A25, both hosting a Ag_{10} cluster in them) along with two 3'-arm fragments (T17–C37 and C26–C37, both hosting a Ag_{1-4} cluster) (Fig. 3d,e). Clearly the breakdown of green-emitting Ag_{13} and Ag_{14} into red-emitting Ag_{10} and non-emissive Ag_{1-4} was responsible for the observed fragmentation-induced colour-switching phenomenon in Subak-1. From the atomically precise structures of Ag_8 and Ag_{16} recently revealed by X-ray crystallography 23,27 , some silvers on the outer face of the AgNC were found loosely associated with the silver core 23 . In our case, three to four silvers might be weakly associated with the rest of the silvers,

which are tightly templated in the 5'-arm. During fragmentation, we believe the nuclease not only cuts the DNA but also separates the loosely bound silvers templated in the 3'-arm from the core tightly encapsulated in the 5'-arm (Fig. 3e). This conjecture was further supported by the observation of the change of the most dominant cluster species in intact Subak-1 from Ag_{13}/Ag_{14} to Ag_{11}/Ag_{12} during long-term storage (>3 weeks), possibly due to the dissociation of weakly bound silvers from the silver core (but the Subak-1 colour remained unchanged, Supplementary Fig. 13).

Following the isotope pattern analysis, Ag₁₃ and Ag₁₀ clusters have four and three neutral Ag atoms (N_0) in their respective cores (Supplementary Figs. 11 and 14–16). It was previously shown that $N_0 = 4$ is a magic number (that is, one of the most abundant AgNC core sizes given by the standard nucleation-and-reduction process)¹⁴, and the AgNC with a magic-number core size is likely to be rod-shaped¹⁶. Besides, many reported AgNCs with $N_0 = 4$ (such as Ag_{10}^{6+}) are green $emitters\,with\,emission\,peaks\,ranging\,from\,540\,to\,550\,nm^{13,14,24},which$ are identical to our Ag_{13}^{9+} emitter. In contrast, since our Ag_{10}^{7+} emitter is made by the nuclease fragmentation process, it is not surprising Ag₁₀⁷⁺ adopts a non-rod shape and has a non-magic-number core $(N_0 = 3)$, with a footprint in the DNA host that is unattainable by the traditional nucleation-and-reduction process (Supplementary Fig. 2). This explains why the Ag_{10}^{7+} is a red emitter while most of the reported Ag₁₀ clusters are green or dark emitters¹³. It is the combinatorial effect (the altered base-cluster interacting footprint and the changed size/ shape of the fragmented AgNC) that leads to the colour-switching phenomenon in Subak. Further footprint studies are needed to support this idea; however, analysing the footprints of AgNCs within DNA fragments is currently challenging due to the difficulty in sample purification (that is, removing all minor species that are not responsible for the observed fluorescence).



 $\label{eq:continuous} \textbf{Fig. 4} | \textbf{Subak optimization via single- and double-mutation tests. a}, \textbf{The} sequence and structure of Subak-seed, with red arrows indicating critical base positions. \textbf{b}, \textbf{c}, \textbf{Green} \textbf{ (b)} and red \textbf{ (c)} fluorescence fold changes compared with the Subak-seed reporter (which was normalized to unity). \textbf{d}, Based on the single-mutation results, 29 double-mutation variants (magenta boxes) were generated and tested. When compared with the Subak-seed, two variants with substantially improved performance were identified: Subak-1 (with T12C/C36G mutations, yellow box) and Subak-2 (with T12C/T17C mutations, blue box). Subak-1 gave 3.2-fold and 1.3-fold increases in green (before fragmentation) and red emissions (after fragmentation), respectively. Subak-2 gave 3.7-fold and 4.7-fold increases$

in green and red emissions, respectively. Though T12C/C36A showed a high increase in the green channel (5.3-fold) with a reasonably good enhancement in the red channel (1.3-fold), it had residual green fluorescence after fragmentation, which led to a lower I_{630}/I_{540} ratio in the ratiometric sensing (Supplementary Fig. 17). $\mathbf{e}-\mathbf{g}$, Fluorescence emission spectra of Subak-seed (\mathbf{e}), Subak-1 (\mathbf{f}) and Subak-2 (\mathbf{g}) under 280 nm excitation. The lines represent the mean values, while the shading represents the standard deviations (n=3 replicates). To preserve the stem-loop structure, when a base in the stem (T11–T17) was mutated, the complementary base was also mutated to maintain the base pair formation.

Optimization of Subak reporters

To optimize Subak reporters, we focused on a 37-nt-long strand that we called 'Subak-seed' (Fig. 4a) and tested its 78 single-mutation (only in arms and stem, Fig. 4b,c) and 29 double-mutation (Fig. 4d) variants. The optimization goal was to increase green and red fluorescence intensities before and after fragmentation, respectively. Some mutations showed a notable increase in green emission (I_{540}) before fragmentation (for example, C4T gave 6.6-fold enhancement), but if their red emissions after fragmentation (I_{630}) were low, they were discarded (Fig. 4b,c). On the basis of these criteria, 9 mutations (red arrows in Fig. 4a and magenta boxes in Fig. 4b,c) were chosen to generate 29 double-mutation variants for further investigation (Fig. 4d).

Two double-mutation variants, Subak-1 and Subak-2 (highlighted by yellow and blue boxes in Fig. 4d), showed notable performance improvement over Subak-seed (Fig. 4e–g). On one hand, T12C substitution was found to give the highest enhancement in red emission (2.3-fold increase as compared with Subak-seed, Fig. 4c). On the other hand, C36A (4.6-fold) and C36G (6.1-fold) substitutions gave the two greatest increases in green emission (Fig. 4b). By combining these and other mutations, we obtained Subak-1 (T12C/C36G, Fig. 4f and Supplementary

Fig. 17) and Subak-2 (T12C/T17C, Fig. 4g) that both showed improved performance over Subak-seed (Fig. 4e). Compared with Subak-1, Subak-2 showed an even stronger fluorescence response to DNase I digestion, which was later used for Cas12a activity detection in the DETECTR assay. Further investigations on the thermodynamics of Subak reporters were then performed using UNAfold software and variable-temperature ESI-MS 29,30 (Supplementary Table 2). Variable-temperature ESI-MS results indicated that the dominant green-emitting species (Ag $_{11-14}$) are stable until 70 °C (Supplementary Fig. 18).

Colour conversion of the two Subak reporters

The observed fragmentation-induced colour-switching phenomenon in Subak could have two possible explanations. First, the green AgNC species in the intact Subak is directly converted into a red AgNC species in the fragments. Second, the green AgNC species is turned into a non-emissive, dark species, while a relatively dark species becomes bright red after fragmentation. Since the gel-purified Subak-1 gave a strong red fluorescence enhancement upon digestion, we concluded that the green AgNC species of Subak-1 is directly converted into a red species (Fig. 5a,b). Since naked DNA and ill-prepared, non-emissive DNA/AgNC species were removed during the gel purification, the

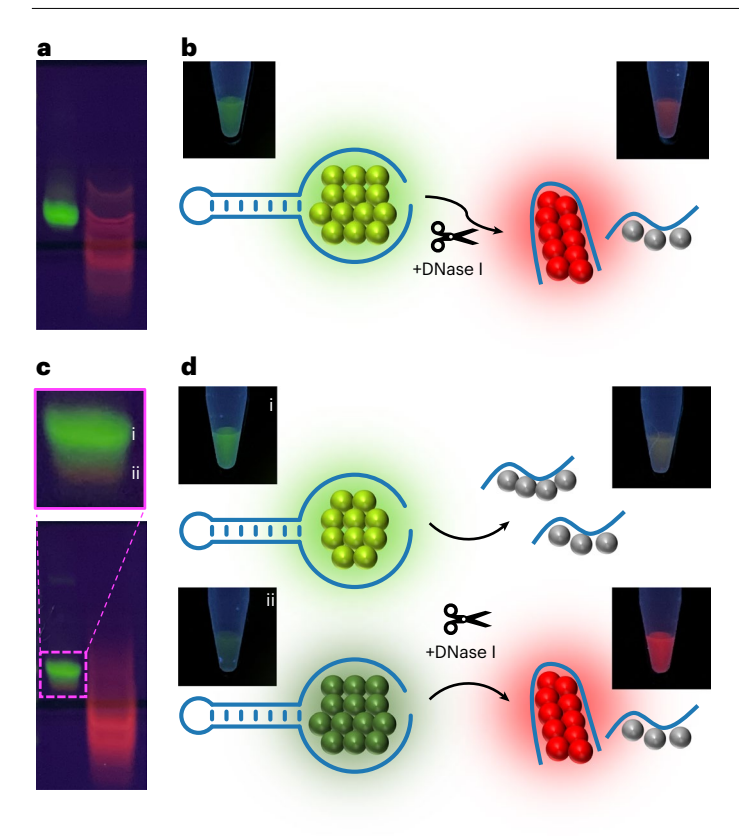


Fig. 5 | **Working principles of Subak-1 and Subak-2.** a,b, The green-emitting band was selectively eluted and mixed with DNase I. The gel-purified Subak-1 reporter showed strong red fluorescence upon digestion. c,d, Although Subak-2 provided higher fluorescence enhancement upon fragmentation, it clearly had a minor, low-emissive DNA/AgNC species that could be eluted from the second band (ii). This low-emissive DNA/AgNC species was solely responsible for the observed red fluorescence after digestion, whereas the green-emitting species from the first band (i) became low emissive after digestion.

purified Subak-1 responded more strongly to nuclease activity than the unpurified Subak-1 (Supplementary Fig. 1).

In contrast, Subak-2 worked in a different way that follows our second hypothesis (Fig. 5c,d). In the gel lane of intact Subak-2, a minor, low-emissive band (ii in Fig. 5c) was observed just below the prominent green band (i in Fig. 5c). ESI-MS identified the low emissive and the strong green bands are Ag₁₃/Ag₁₄ and Ag₁₀/Ag₁₁, respectively (Supplementary Fig. 19). The relatively dark species (Ag₁₃/Ag₁₄, ii in Fig. 5c) was responsible for the strong red emission observed after fragmentation, while the green-emitting species (Ag₁₀/Ag₁₁, i in Fig. 5c) became low emissive after digestion (Fig. 5d). Thus, unlike Subak-1, which refers to a single AgNC species (Ag₁₃ or Ag₁₄) that is directly converted into a red species (Ag₁₀) upon fragmentation, Subak-2 collectively represents two AgNC species: one shows green-to-dark conversion while the other exhibits dim-green-to-red conversion upon fragmentation. While both Subak-1 and Subak-2 change from green to red upon fragmentation, the principles behind the observed phenomenon are different. Despite the difference in their conversion principles, both Subak reporters support ratiometric sensing of DNase I activity.

Subak-2 in amplification-free DETECTR assay

Although Subak-1 works well for detecting DNase I activity, it does not respond strongly to activated Cas12a (Supplementary Fig. 20). In contrast, Subak-2 responds strongly to the Cas12a *trans* cleavage activity (Fig. 6). It is possible that Subak-2 offers more favourable cleavage sites for the Cas12a nuclease to act on (Supplementary Fig. 21). Once activated by a severe acute respiratory syndrome coronavirus 2

(SARS-CoV-2) complementary DNA strand (Supplementary Table 3), Cas12a trans cleaved Subak-2, turning the solution from green to red under UV excitation (Fig. 6a). Compared with the reactions where DNaseAlert was used as a reporter (Fig. 6b), Subak-2 provided a comparable LOD (1.19 pM versus 0.54 pM, Fig. 6c-e) and dynamic range (10³) under the same reaction conditions in an amplification-free assay. Due to the ratiometric sensing capability of Subak-2, the fold change of Subak-2 was 15 times higher than that of DNaseAlert at one-sixtieth of the cost (Fig. 6e and Supplementary Table 4). The only drawback of Subak-2 is its slower reaction velocity by activated Cas12a (36 times slower than that of DNaseAlert³¹; Fig. 6e, Supplementary Fig. 22 and 23 and Supplementary Equation 1). This might be because Cas12a trans cleaves single-stranded DNA more effectively than double-stranded DNA (dsDNA)^{32,33}, and, similar to Subak-1, Subak-2's preferred cleavage sites are in the stem (Supplementary Fig. 21). The ESI-MS results also confirmed that the Ag₁₃ to Ag₁₀ conversion was behind the dim-green-to-red conversion of the AgNC species eluted from the second gel band (2 in Fig. 5c), upon Cas12a fragmentation (Supplementary Figs. 24-26).

Conclusions

We previously reported the guanine-induced fluorescence-enhancement property of dark AgNCs templated in DNA 9,22,34, creating a unique class of activatable molecular probes termed nanocluster beacons (NCBs) for the detection of single-nucleotide polymorphisms¹², topoisomerase activities³⁵ and DNA methylation²¹. In NCBs, when the additional nucleobases (mainly guanines) are brought close to the dark AgNC, they turn on its fluorescence. Although NCBs have made a substantial impact in the molecular sensing field^{36,37}, how NCBs are transformed from a dark species into a bright species is still a mystery. In contrast, here we have strong evidence that Subak reporters are converted from one species (for example, a green species) into another (for example, a red species) due to the subtractive process (for example, Ag₁₃/Ag₁₄ to Ag_{10}). Although it is believed that the number of neutral Ag atoms in a AgNC core (N_0) is a key determinant of the AgNC colour ^{14,38}, there was no previously known well-controlled method that can convert a AgNC of a predefined core size/shape stabilized by nucleobase ligands (not by small-molecule ligands³⁹) into another AgNC species with a different core size/shape and emission colour. This is the first report to demonstrate such a possibility. Whereas NCBs work by bringing additional nucleobases close to AgNCs to activate them. Subak reporters work in the completely opposite way, making them the 'inverse' NCBs (i-NCBs).

Although the name 'Subak' (meaning watermelon in Korean) implies a green-to-red conversion upon cutting (most watermelons are green on the outside and red in the inside), Subak reporters showing other types of colour conversions are also discovered by us (for example, Subak-3 showed a green-to-yellow colour conversion upon fragmentation, Supplementary Fig. 4). In general, if a DNA/AgNC probe's colour conversion mechanism is due to the subtractive process of AgNCs during fragmentation, it should be called a Subak reporter. We also showed that Subak is not limited to detecting DNase activity but can also be used for detecting RNase detection (by incorporating ribonucleotides in the reporter design, Supplementary Fig. 27).

Whereas almost all digestion-and-light-up reporters available today are FRET reporters (with a few exceptions⁴⁰), Subak reporters offer a low-cost, non-FRET probe with ratiometric sensing capability for the community to use. Our results not only demonstrate that DNA/AgNC probes can be versatile reporters for detecting nuclease activities but also provide insights into the interactions between nucleases and metallo-DNA nanomaterials. Further improvement of Subak will facilitate the detection of various targets including small molecules and RNA, in combination with RNA-cleaving DNAzymes^{41,42} and RNA-targeting Cas effectors such as Cas13 (ref. 5).

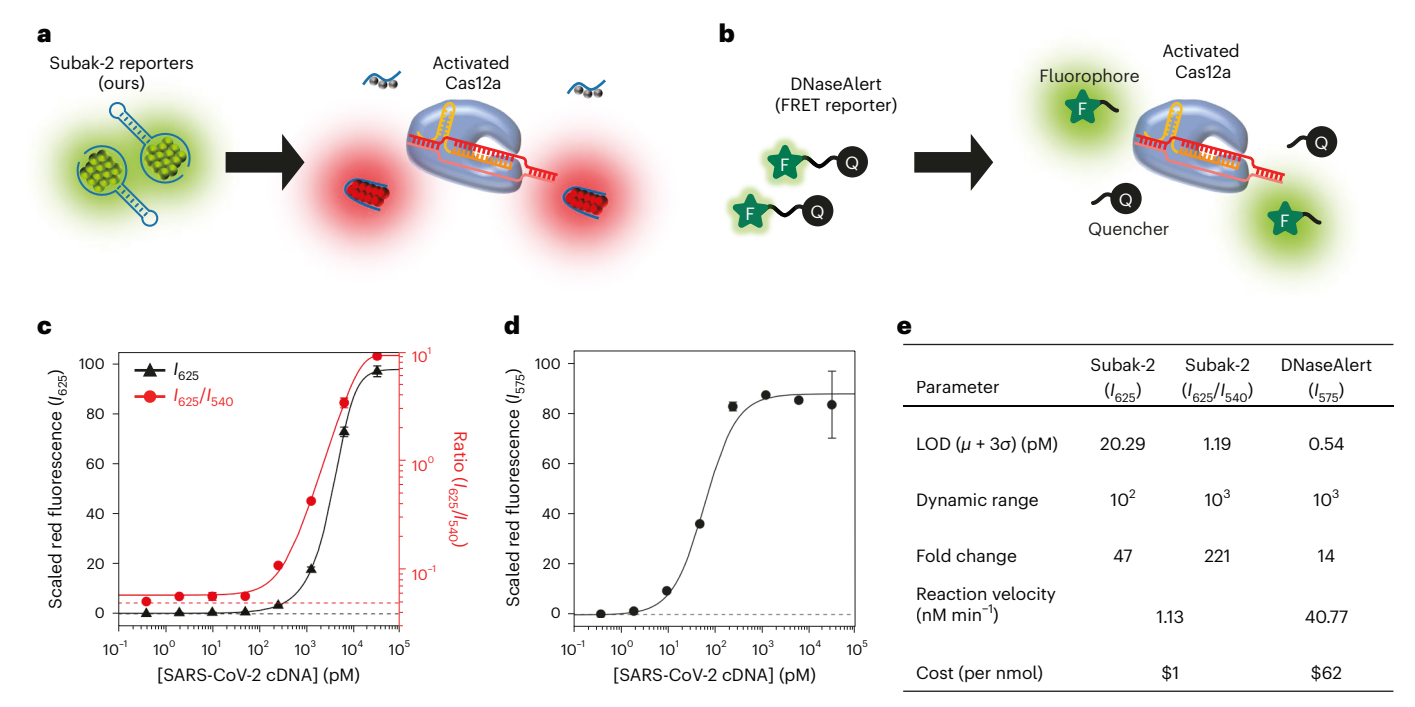


Fig. 6 | Subak-2 reporting synthetic SARS-CoV-2 cDNA in amplification-free DETECTR assay. a, b, Schematic diagrams of Subak-2 and FRET reporter DNaseAlert in DETECR assay. **c,** Subak-2 response to activated Cas12a in the presence of various amounts of SARS-CoV-2 cDNA. Both single-colour (I_{625} , black line) and ratiometric sensing (I_{625} / I_{540} , red line) results were obtained. The green fluorescence (I_{540}) was measured at 540 nm under 480 nm excitation, while the

red fluorescence (I_{625}) was measured at 625 nm under 565 nm excitation. **d**, Single-colour (I_{575}) DNaseAlert response to activated Cas12a under 535 nm excitation. Sigmoidal regression curves were fitted using a 5-PL regression (Supplementary Equation 2). The dots represent the mean values, while the error bars represent the standard deviations (n=3 replicates). **e**, Comparison between Subak-2 and DNaseAlert in five sensing parameters.

Online content

Any methods, additional references, Nature Portfolio reporting summaries, source data, extended data, supplementary information, acknowledgements, peer review information; details of author contributions and competing interests; and statements of data and code availability are available at https://doi.org/10.1038/s41565-024-01612-6.

References

- Notomi, T. et al. Loop-mediated isothermal amplification of DNA. Nucleic Acids Res. 28, e63–e63 (2000).
- Piepenburg, O., Williams, C. H., Stemple, D. L. & Armes, N. A. DNA detection using recombination proteins. *PLoS Biol.* 4, e204 (2006).
- Fozouni, P. et al. Amplification-free detection of SARS-CoV-2 with CRISPR-Cas13a and mobile phone microscopy. Cell 184, 323–333 (2021).
- Chen, J. S. et al. CRISPR-Cas12a target binding unleashes indiscriminate single-stranded DNase activity. Science 360, 436-439 (2018).
- Gootenberg, J. S. et al. Nucleic acid detection with CRISPR-Cas13a/C2c2. Science 356, 438–442 (2017).
- Holland, P. M., Abramson, R. D., Watson, R. & Gelfand, D. H. Detection of specific polymerase chain reaction product by utilizing the 5'-3' exonuclease activity of *Thermus aquaticus* DNA polymerase. *Proc. Natl Acad. Sci. USA* 88, 7276–7280 (1991).
- Broughton, J. P. et al. CRISPR-Cas12-based detection of SARS-CoV-2. Nat. Biotechnol. 38, 870–874 (2020).
- 8. Marras, S. A., Kramer, F. R. & Tyagi, S. Efficiencies of fluorescence resonance energy transfer and contact-mediated quenching in oligonucleotide probes. *Nucleic Acids Res.* **30**, e122–e122 (2002).
- Yeh, H.-C., Sharma, J., Han, J. J., Martinez, J. S. & Werner, J. H. A. DNA-silver nanocluster probe that fluoresces upon hybridization. *Nano Lett.* 10, 3106–3110 (2010).

- 10. O'Neill, P. R., Gwinn, E. G. & Fygenson, D. K. UV excitation of DNA stabilized Ag cluster fluorescence via the DNA bases. *J. Phys. Chem.* C **115**, 24061–24066 (2011).
- Petty, J. T., Zheng, J., Hud, N. V. & Dickson, R. M. DNA-templated Ag nanocluster formation. J. Am. Chem. Soc. 126, 5207–5212 (2004).
- Yeh, H.-C. et al. A fluorescence light-up Ag nanocluster probe that discriminates single-nucleotide variants by emission color. J. Am. Chem. Soc. 134, 11550–11558 (2012).
- Blevins, M. S. et al. Footprints of nanoscale DNA-silver cluster chromophores via activated-electron photodetachment mass spectrometry. ACS Nano 13, 14070-14079 (2019).
- Copp, S. M. et al. Magic numbers in DNA-stabilized fluorescent silver clusters lead to magic colors. J. Phys. Chem. Lett. 5, 959–963 (2014).
- He, C., Goodwin, P. M., Yunus, A. I., Dickson, R. M. & Petty, J. T. A split DNA scaffold for a green fluorescent silver cluster. *J. Phys. Chem.* C 123, 17588–17597 (2019).
- Schultz, D. et al. Evidence for rod-shaped DNA-stabilized silver nanocluster emitters. Adv. Mater. 25, 2797–2803 (2013).
- Petty, J. T. et al. Optical sensing by transforming chromophoric silver clusters in DNA nanoreactors. *Anal. Chem.* 84, 356–364 (2012).
- Chen, J. et al. CRISPR/Cas precisely regulated DNA-templated silver nanocluster fluorescence sensor for meat adulteration detection. J. Agric. Food Chem. 70, 14296–14303 (2022).
- Lee, C. Y., Park, K. S., Jung, Y. K. & Park, H. G. A label-free fluorescent assay for deoxyribonuclease I activity based on DNA-templated silver nanocluster/graphene oxide nanocomposite. *Biosens. Bioelectron.* 93, 293–297 (2017).
- Kuo, Y. A. et al. Massively parallel selection of nanocluster beacons. Adv. Mater. 34, e2204957 (2022).

- Chen, Y.-A. et al. Nanocluster beacons enable detection of a single N⁶-methyladenine. J. Am. Chem. Soc. 137, 10476–10479 (2015).
- 22. Obliosca, J. M. et al. A complementary palette of nanocluster beacons. ACS Nano 8, 10150–10160 (2014).
- Cerretani, C., Kanazawa, H., Vosch, T. & Kondo, J. Crystal structure of a NIR-emitting DNA-stabilized Ag₁₆ nanocluster. *Angew. Chem. Int. Ed.* 58, 17153–17157 (2019).
- Petty, J. T. et al. A DNA-encapsulated silver cluster and the roles of its nucleobase ligands. J. Phys. Chem. C 122, 28382–28392 (2018).
- Koszinowski, K. & Ballweg, K. A highly charged Ag₆⁴⁺ core in a DNA-encapsulated silver nanocluster. *Chem. Eur. J.* 16, 3285–3290 (2010).
- Gonzalez-Rosell, A. et al. Chloride ligands on DNA-stabilized silver nanoclusters. J. Am. Chem. Soc. 145, 10721–10729 (2023).
- 27. Huard, D. J. et al. Atomic structure of a fluorescent Ag_8 cluster templated by a multistranded DNA scaffold. *J. Am. Chem. Soc.* **141**, 11465–11470 (2018).
- Markham, N. R. & Zuker, M. UNAFold: software for nucleic acid folding and hybridization. *Methods Mol. Biol.* 453, 3–31 (2008).
- 29. Cong, X. et al. Determining membrane protein-lipid binding thermodynamics using native mass spectrometry. *J. Am. Chem.* Soc. **138**, 4346–4349 (2016).
- McCabe, J. W. et al. Variable-temperature electrospray ionization for temperature-dependent folding/refolding reactions of proteins and ligand binding. *Anal. Chem.* 93, 6924–6931 (2021).
- Ramachandran, A. & Santiago, J. G. CRISPR enzyme kinetics for molecular diagnostics. *Anal. Chem.* 93, 7456–7464 (2021).
- Nguyen, L. T., Smith, B. M. & Jain, P. K. Enhancement of trans-cleavage activity of Cas12a with engineered crRNA enables amplified nucleic acid detection. *Nat. Commun.* 11, 4906 (2020).
- Nalefski, E. A. et al. Kinetic analysis of Cas12a and Cas13a RNA-guided nucleases for development of improved CRISPR-based diagnostics. iScience 24, 102996 (2021).

- Yeh, H.-C., Sharma, J., Han, J. J., Martinez, J. S. & Werner, J. H. A beacon of light. *IEEE Nanotechnol. Mag.* 5, 28–33 (2011).
- Juul, S. et al. Nanocluster beacons as reporter probes in rolling circle enhanced enzyme activity detection. *Nanoscale* 7, 8332–8337 (2015).
- 36. Ge, L., Sun, X., Hong, Q. & Li, F. Ratiometric nanocluster beacon: a label-free and sensitive fluorescent DNA detection platform. ACS Appl. Mater. Interfaces 9, 13102–13110 (2017).
- Suo, T. et al. A versatile turn-on fluorometric biosensing profile based on split aptamers-involved assembly of nanocluster beacon sandwich. Sens. Actuators B 324, 128586 (2020).
- Gwinn, E., Schultz, D., Copp, S. M. & Swasey, S. DNA-protected silver clusters for nanophotonics. *Nanomaterials* 5, 180–207 (2015).
- Zou, X., Kang, X. & Zhu, M. Recent developments in the investigation of driving forces for transforming coinage metal nanoclusters. Chem. Soc. Rev. 52, 5892–5967 (2023).
- 40. Leytus, S. P., Melhado, L. L. & Mangel, W. F. Rhodamine-based compounds as fluorogenic substrates for serine proteinases. *Biochem. J.* **209**, 299–307 (1983).
- 41. Broto, M. et al. Nanozyme-catalysed CRISPR assay for preamplification-free detection of non-coding RNAs. *Nat. Nanotechnol.* **17**, 1120–1126 (2022).
- 42. Hu, Q. et al. DNAzyme-based faithful probing and pulldown to identify candidate biomarkers of low abundance. *Nat. Chem.* **16**, 122–131 (2023).

Publisher's note Springer Nature remains neutral with regard to jurisdictional claims in published maps and institutional affiliations.

Springer Nature or its licensor (e.g. a society or other partner) holds exclusive rights to this article under a publishing agreement with the author(s) or other rightsholder(s); author self-archiving of the accepted manuscript version of this article is solely governed by the terms of such publishing agreement and applicable law.

© The Author(s), under exclusive licence to Springer Nature Limited 2024

Methods

DNA/AgNC preparation

The oligonucleotides (Integrated DNA Technologies, IDT) were suspended at 500 µM in DNase-free water and then thawed in water at 70 °C for 2 min and cooled for at least 5 min. To make 1 ml of solution, 80 ul of 500 µM DNA was added to 100 ml of 200 mM sodium phosphate buffer (SPB, pH 7.4) with 748 µl of nuclease-free water. The solution was then mixed with 48 µl of 10 mM silver nitrate (AgNO₃, cat. no. 204390, Sigma-Aldrich) solution, and then vortexed and centrifuged for 1 min at 14,000g. After equilibration for 20 min, the mixture was reduced with 24 µl of 10 mM freshly prepared sodium borohydride (NaBH₄, cat. no. 480886, Sigma-Aldrich) to form the DNA/AgNCs. The solution was then vortexed and centrifuged again for 1 min at 14,000g. The final concentrations were 40 uM DNA, 20 mM SPB, 480 uM AgNO₃ and 240 µM NaBH₄. The product was stored at 4 °C for at least 1 week before further analysis. SPB was prepared by mixing sodium phosphate dibasic anhydrous (Na₂HPO₄, cat. no. S375-500, Fisher Scientific) with sodium phosphate monobasic monohydrate (NaH₂PO₄•H₂O, cat. no. S468-500, Fisher Scientific).

Optical characterization

Three-dimensional excitation–emission matrices were collected on a fluorometer (FluoroMax-4, Horiba) using a quartz cuvette (cat. no. 16.100F-Q-10/Z15, Sterna Cells). The scan ranges for both excitation and emission were set to be 400–800 nm in increments of 5 nm. The slit size and integration time were 5 nm and 0.1 s, respectively. Unless otherwise stated, 120 μl of 1 μM sample was used for one measurement. The acquired data were post-processed and visualized using a Python script.

All other fluorescence data were collected using a plate reader (SpectraMax i3, Molecular Devices) and a half-area UV transparent 96-well microplate (cat. no. 675801, Greiner Bio-One). The bandwidths for excitation and emission were 9 nm and 15 nm, respectively. The microplate was shaken for 2 s between reads. Each read was averaged with 20 lamp flashes. The read height was optimized before measurement. Each well was filled with 80 μ l of 500 nM sample. For emission spectrum scanning, the increment was 5 nm; for a kinetic read, the data were collected every 2 min at 37 °C.

Absorption data were also collected using the same plate reader and microplate. For a kinetic read, $80~\mu l$ of $2~\mu M$ sample was loaded into each well. The data were measured every 2~min at 37~C. For spectrum scanning, the absorption was scanned from 400~to 700 nm in increments of 5~nm. The concentration of all DNA-related samples was quantified and validated using a spectrophotometer (NanoDrop One Microvolume UV–Visible Spectrophotometer, Thermo Fisher Scientific).

Gel electrophoresis

Handcast polyacrylamide gels (20–25%) were prepared. For example, 16 ml of 20% gel was prepared as follows: 6.224 ml of nuclease-free water was added to 8 ml of 40% acrylamide solution (cat. no. HC2040), and the solution was mixed with 1.6 ml of $10\times$ Tris-borate-ethylenediaminetetraacetic acid (TBE) buffer (cat. no. BP1333-1, Fisher Scientific). Then, 16 µl of N, N, N-tetramethylethylenediamine (TEMED) (cat. no. HC2006) was added. After mixing 160 µl of 10% ammonium persulfate (cat. no. HC2005), the gel solution was quickly poured into an empty gel cassette (cat. no. NC2010) installed in a customized handcast station. A gel comb (cat. nos. NC3002, NC3010 and NC3012) was then slowly inserted, and the gel was polymerized for >30 min at room temperature. The gel can be used immediately or stored at 4 °C with a damp paper towel wrapped for future use. Sixteen millilitres of gel solution was sufficient for preparing two gels.

Gel electrophoresis was conducted using XCell SureLock Mini-Cell (cat. no. El0001) connected to a power supply (cat. no. PS0120). Sample (20 µl) was loaded into each well of a precast gel. The sample was loaded

with 10× TBE loading buffer, which was prepared by mixing 2 ml of 10× TBE buffer with 3 g Ficoll type 400 (cat. no. F10400-10.0, Research Products International) and nuclease-free water to 10 ml. The sample was concentrated up to 250 µM using a 3 kDa molecular weight cut-off (MWCO) centrifugal filter (cat. no. UFC5003, Sigma-Aldrich) if necessary. Every gel contained at least one ladder lane using a DNA oligo standard (cat. no. 51-05-15-01, IDT) labelled with SYBR gold (cat. no. S11494, Thermo Fisher Scientific). Then, the gel was run at 160 V for 150 min in 1× TBE buffer unless stated otherwise and visualized using a UV transilluminator for true colour images (model no. GV4L20X20, Syngene) or a gel imager (Typhoon FLA 9500, GE Healthcare) for false colour images. The UV transilluminator is equipped with a 365 nm UV lamp, and the true colour UV photos were taken by a iPhone 12 Pro (Apple) using Adobe Lightroom (ISO 500, 1/40 s for shutter speed and f/1.6 aperture) in a custom-built imaging system (Supplementary Fig. 28). For false colour images, long-pass emission filters installed in the gel imager were used with the cut-on wavelengths of 510 nm and 575 nm for 473 nm and 532 nm in excitation wavelengths, respectively. The photomultiplier tube gain was 500 V and the pixel size was 50 µm. Materials for gel electrophoresis $were \, purchased \, from \, Thermo \, Fisher \, Scientific \, unless \, stated \, otherwise.$

Gel purification

Subak reporters were purified by a modified crush-and-soak method using high-percentage PAGE (Supplementary Fig. 7). Then, 350 µl of 150 µM Subak reporters were loaded into a 24% handcast PAGE gels with a two-dimensional well comb. The loading sample included 35 μl of the aforementioned 10× loading buffer. After running at 160 V for 400 min, the gel was visualized under a UV transilluminator, and then a fluorescent gel slab was cut and eluted using a gel cutter (cat. no. 10048-876, VWR). This eluted gel was crushed as small as possible, and then soaked in 20 mM SPB (pH 7.4) overnight. This solution was transferred to a 0.45 µm polyvinylidene difluoride column filter (cat. no. F2517-6, Thermo Fisher Scientific), and then centrifuged at 7,000g for 30 min to remove any remaining gel fragments. The concentrate was quantified by measuring A_{260} by a spectrophotometer and stored at 4 °C for future use otherwise used immediately. By doing so, a large amount of DNA/AgNCs could be collected. One gel yielded >400 µl of 50 µM Subak reporters given that the synthetic yield was 40% (Supplementary Fig. 9).

DNase I digestion

DNase I and 10× DNase reaction buffer were purchased from New England Biolabs (cat. nos. M0303S and B0303S, respectively). The 1× reaction buffer was composed of 10 mM Tris–HCl, 2.5 mM MgCl $_2$ and 0.5 CaCl $_2$ (pH 7.6). The specific activity of DNase I is approximately 20,000 units mg $^{-1}$, by which the stock concentration was converted to 0.1 µg µl $^{-1}$. A fivefold serial dilution of DNase I was conducted for DNase quantification. DNase I quantification experiment was started by mixing 8 µl of 10× buffer with 54 µl of nuclease-free water in a 96-well plate. Then, 8 µl of 5 µM reporters were then loaded and mixed with a microplate centrifuge (cat. no. 14-955-300, Fisher Scientific). Next, 8 µl of 10× DNase I was mixed and incubated at 37 °C for 20 min for an endpoint read and different times for a kinetic read.

LOD calculation

Assay data were fitted using a five-parameter logistic (5-PL) equation (Supplementary Equation 2). Raw data and curve fitting parameters are reported in Source data. Using this fitted curve, the LOD was then determined by the concentration that gives the mean + 3 s.d. of the control (dashed lines).

MS

Before nanoelectrospray ionization (nESI)–MS, solutions containing 10 µM Subak reporters in 10 mM ammonium acetate were purified using a Micro Bio-Spin P-6 Gel Column (Bio-Rad). Octylamine

was added to the solution at a concentration of approximately 0.1% (vol/vol), Samples were infused into an Orbitrap Fusion Lumos mass spectrometer (Thermo Fisher Scientific) using Au/Pd-coated borosilicate emitters fabricated in-house for nESI. Mass spectra were collected in negative ion mode between m/z 400 and 2,500 using a resolving power of 120,000 at m/z 200, an automatic gain control target of 1 × 10⁶ charges, and an ionization voltage of 550-600 V. For experiments involving variable temperature ESI (vT-ESI), a home-built vT-ESI source was interfaced with a Q Exactive HF-X Biopharma Orbitrap Mass Spectrometer (Thermo Fisher Scientific) that was modified with a 193 nm excimer laser^{43,44}. The design of the home-built temperature vT-ESI source used in the experiments was described previously³⁰. Temperature-dependent mass spectra of the Subak-1 reporter were collected at a temperature range of 20–100 °C in increments of 10 °C. Mass spectra were collected in negative ion mode for 1 min at each temperature point using a resolving power of 120,000 at m/z 200, automatic gain control of 1×10^6 , and ionization voltage of 750 V. The mass spectrometer was operated in high mass range mode with a trapping gas setting of 1 (a.u.). All mass spectra were deconvoluted using Xtract in FreeStyle version 1.8 (Thermo Fisher Scientific). The following deconvolution parameters were applied: signal-to-noise threshold of 3, fit factor of 80% and remainder threshold of 25%. Theoretical isotopic distributions were calculated using Xcalibur Qual Browser (Thermo Fisher Scientific). All mass spectra were interpreted and annotated manually with the aid of Mongo Oligo Mass Calculator v2.06. The mass spectrometer was calibrated using a mixture of components designed for the negative ionization mode to ensure high mass accuracy (for example, ≤10 ppm error).

In vitro CRISPR-Cas reaction

Lachnospiraceae bacterium (LbCas12a) and rCutSmart buffer were purchased from New England Biolabs. First, 100 μl of 10 μM ribonucleoprotein (RNP) complexes were made by mixing 20 µl of nuclease-free water, 10 μl of 10× rCutSmart buffer (cat. no. B6004S), 10 μl of 100 μM stock LbCas12a (cat. no. M0653T) and 60 µl of 20 µM guide RNA (gRNA, IDT). The final ratio between Cas12a and gRNA was 1:1.2 to fully form RNPs. The 1× buffer components were 50 mM potassium acetate, 20 mM Tris-acetate, 10 mM magnesium acetate and 100 μg ml⁻¹ recombinant albumin (pH 7.9). After 10 min at room temperature, the RNP solution was activated by loading dsDNA of target strands (IDT, Supplementary Table 3) of different concentrations in a final reaction volume of 60 ul. which consisted of 42 μl of nuclease-free water, 6 μl of 10× buffer, 6 μl of 10 μM RNP and 6 μl of 10× target strands. This solution was then incubated at 37 °C for 20 min before mixing with 500 nM reporters. Target strands in the no-target control were substituted with nuclease-free water. For 80 μl of trans cleavage reaction, 8 μl of 10× buffer, 8 μl of 1 μM activated RNPs and 8 μl of 5 μM reporters were mixed with 56 μl of nuclease-free water. The final concentrations were 100 nM Cas12a, 120 nM gRNA and 500 nM reporters with various concentrations of target strands.

We compared Subak-1 and Subak-2 probes with the commercially available FRET probes, DNaseAlert (cat. no. 11-04-02-04, IDT). For three-dimensional fluorescence measurements using a fluorometer (Fluoromax-4, Horiba), the solution was incubated at 37 °C for 30 min. For kinetic and titration analysis, the fluorescence was monitored in a plate reader (SpectraMax i3, Molecular Devices). To validate that Subak-2 reporters were specifically cleaved when gRNA was matched with the pair target strands, another dsDNA target/gRNA pair was used (Supplementary Table 3 and Supplementary Fig. 29).

The fold change was calculated by dividing the fluorescence or the fluorescence ratio in the presence of target strands (31.25 nM) by the fluorescence or the ratio in the control sample (without target strands) after 60 min incubation (Figs. 1e and 6e).

Reporting summary

Further information on research design is available in the Nature Portfolio Reporting Summary linked to this article.

Data availability

Source data are provided with this paper and available online at https://doi.org/10.5281/zenodo.10394146.

Code availability

The code designed for data collection and analysis of this study is available online at https://doi.org/10.5281/zenodo.10394146.

References

- 43. Fort, K. L. et al. Implementation of ultraviolet photodissociation on a benchtop Q exactive mass spectrometer and its application to phosphoproteomics. *Anal. Chem.* **88**, 2303–2310 (2016).
- 44. Sanders, J. D. et al. Enhanced ion mobility separation and characterization of isomeric phosphatidylcholines using absorption mode Fourier transform multiplexing and ultraviolet photodissociation mass spectrometry. *Anal. Chem.* 94, 4252–4259 (2022).

Acknowledgements

This work was supported by the National Science Foundation grants (CBET2029266 to H.-C.Y. and J.S.B., and CBET2041340 to M.J.K.) and the National Institutes of Health grant (EY033106 to H.-C.Y.). The authors thank I. C. Santos for improving the ESI–MS analysis workflow on DNA/AgNCs, S. Kim for her assistance in the RNase A experiment and A. Yeh for his assistance in the revision.

Author contributions

S.H. and H.-C.Y. conceived the project and designed the experiments. S.H. designed the DNA sequences for Subak reporters and mutation tests to optimize the reporters. S.H. developed a gel-purification method to purify DNA/AgNCs. S.H. performed DNase I, Cas12a and RNase A experiments. A.T.L. and J.M. performed fluorescence measurements and developed a Python code for excitation–emission matrices analysis. S.H. and J.N.W. prepared the samples for MS measurements. J.N.W. performed MS measurements and data analysis with assistance from S.W.J.S. and J.S.B. J.S.B. supervised all MS experiments and data analysis. T.D.N., Y.-A.K. and Y.-I.C. collected the absorption data. Y.H. and A.-T.N. checked the buffer compatibility for DNase I digestion and in vitro CRISPR–Cas reaction. M.L.G. and M.J.K. optimized the AgNC synthesis. S.H. and H.-C.Y. wrote the article with input from all authors. H.-C.Y. supervised the project.

Competing interests

The authors declare no competing interests.

Additional information

Supplementary information The online version contains supplementary material available at https://doi.org/10.1038/s41565-024-01612-6.

 $\begin{tabular}{ll} \textbf{Correspondence and requests for materials} should be addressed to \\ \textbf{Hsin-Chih Yeh.} \end{tabular}$

Peer review information *Nature Nanotechnology* thanks the anonymous reviewers for their contribution to the peer review of this work.

Reprints and permissions information is available at www.nature.com/reprints.

nature portfolio

| Corresponding author(s): | Hsin-Chih Yeh |
|----------------------------|---------------|
| Last updated by author(s): | Soonwoo Hong |

Reporting Summary

Nature Portfolio wishes to improve the reproducibility of the work that we publish. This form provides structure for consistency and transparency in reporting. For further information on Nature Portfolio policies, see our <u>Editorial Policies</u> and the <u>Editorial Policy Checklist</u>.

Please do not complete any field with "not applicable" or n/a. Refer to the help text for what text to use if an item is not relevant to your study. For final submission: please carefully check your responses for accuracy; you will not be able to make changes later.

For all statistical analyses, confirm that the following items are present in the figure legend, table legend, main text, or Methods section

| $\overline{}$ | | | | | | |
|---------------|---|-----------------------|----|-----|-----|-----|
| Š | + | \neg | 11 | ct | ۲ı. | CS |
| - 0 | | $\boldsymbol{\alpha}$ | | , n | | , , |

| n /a | Cantingo | ,,,,,,,,,,,, | | | |
|------|--|---|--|--|--|
| n/a | /a Confirmed | | | | |
| | The exact sample size (n) for each experimental group/condition, given as a discrete number and unit of measurement | | | | |
| | 🔀 A statemei | nt on whether measurements were taken from distinct samples or whether the same sample was measured repeatedly | | | |
| X | | ical test(s) used AND whether they are one- or two-sided on tests should be described solely by name; describe more complex techniques in the Methods section. | | | |
| X | A descripti | on of all covariates tested | | | |
| | X A descripti | on of any assumptions or corrections, such as tests of normality and adjustment for multiple comparisons | | | |
| | A full desci | ription of the statistical parameters including central tendency (e.g. means) or other basic estimates (e.g. regression coefficient) cion (e.g. standard deviation) or associated estimates of uncertainty (e.g. confidence intervals) | | | |
| X | For null hypothesis testing, the test statistic (e.g. <i>F</i> , <i>t</i> , <i>r</i>) with confidence intervals, effect sizes, degrees of freedom and <i>P</i> value noted Give <i>P</i> values as exact values whenever suitable. | | | | |
| X | For Bayesia | an analysis, information on the choice of priors and Markov chain Monte Carlo settings | | | |
| X | For hierard | chical and complex designs, identification of the appropriate level for tests and full reporting of outcomes | | | |
| X | Estimates | of effect sizes (e.g. Cohen's d, Pearson's r), indicating how they were calculated | | | |
| | I | Our web collection on statistics for biologists contains articles on many of the points above. | | | |
| | | | | | |
| So | ftware and | d code | | | |
| Poli | cy information a | bout <u>availability of computer code</u> | | | |
| Da | ata collection | The excitation-emission matrix were acquired using Fluoremax-4. All other fluorescence and absorbance data were obtained using SpectraMax i3. Gel images were taken either by iPhone 12pro using Adobe Lightroom or by GE Typhoon FLA 9500. Syngene GV4L transilluminator was used as a UV excitation source, The concentration of DNAs was measured using NanoDrop One Microvolume UV-Vis spectrophotometer. | | | |
| Da | ata analysis | Fluorescence data were analyzed using Python (3.8) and MATLAB (R2023a), Gel data were analyzed using ImageJ (1,54a), Statistical analysis was performed using MATLAB (R2023a) with Curve Fitting Toolbox. | | | |
| | For manuscripts utilizing custom algorithms or software that are central to the research but not yet described in published literature, software must be made available to editors and reviewers. We strongly encourage code deposition in a community repository (e.g. GitHub). See the Nature Portfolio guidelines for submitting code & software for further information. | | | | |

Data

Policy information about availability of data

All manuscripts must include a <u>data availability statement</u>. This statement should provide the following information, where applicable:

- Accession codes, unique identifiers, or web links for publicly available datasets
- A description of any restrictions on data availability
- For clinical datasets or third party data, please ensure that the statement adheres to our $\underline{\text{policy}}$

The data reported in this paper and Source data are available in Supplementary Information and Supplementary Data.

| Research invo | olving human participants, their data, or biological material |
|---------------|---|
| | bout studies with |

Timing

Data exclusions

Non-participation

Randomization

| Ecological, e | volutionary & environmental sciences study design |
|--|--|
| | these points even when the disclosure is negative. |
| Study description | |
| Research sample | |
| Sampling strategy | |
| Data collection | |
| Timing and spatial scale | |
| Data exclusions | |
| Reproducibility | |
| Randomization | |
| Blinding | |
| Did the study involve field | l work? ☐ Yes ☒ No |
| Field work, collect | cion and transport |
| Field conditions | |
| Location | |
| Access & import/export | |
| Disturbance | |
| We require information from a | r specific materials, systems and methods uthors about some types of materials, experimental systems and methods used in many studies. Here, indicate whether each material, vant to your study. If you are not sure if a list item applies to your research, read the appropriate section before selecting a response. |
| Materials & experime | ntal systems Methods |
| n/a Involved in the study | n/a Involved in the study |
| Antibodies | ChIP-seq |
| Eukaryotic cell lines | Flow cytometry |
| Palaeontology and a Animals and other o | —— |
| Clinical data | |
| Dual use research of | concern |
| Plants | |

Antibodies

| Antibodies used | |
|-----------------|--|
| Validation | |

| Eukaryotic cell line | 25 |
|---|---|
| Policy information about <u>ce</u> | Il lines and Sex and Gender in Research |
| Cell line source(s) | |
| Authentication | |
| Mycoplasma contamination | on C |
| Commonly misidentified I (See <u>ICLAC</u> register) | nes |
| Palaeontology and | d Archaeology |
| Specimen provenance | |
| Specimen deposition | |
| Dating methods | |
| Tick this box to confirm | n that the raw and calibrated dates are available in the paper or in Supplementary Information. |
| Ethics oversight | |
| Note that full information on th | ne approval of the study protocol must also be provided in the manuscript. |
| Animals and other | research organisms |
| Policy information about <u>stu</u> <u>Research</u> | udies involving animals; ARRIVE guidelines recommended for reporting animal research, and Sex and Gender in |
| Laboratory animals | |
| Wild animals | |
| Reporting on sex | |
| Field-collected samples | |
| Ethics oversight | |
| Note that full information on th | ne approval of the study protocol must also be provided in the manuscript. |
| | |
| Clinical data | |
| Policy information about <u>cli</u> | nical studies with the ICMJE guidelines for publication of clinical research and a completed CONSORT checklist must be included with all submissions. |
| Clinical trial registration | |
| Study protocol | |
| Data collection | |
| Outcomes | |

Dual use research of concern

Policy information about <u>dual use research of concern</u>

Hazards

Could the accidental, deliberate or reckless misuse of agents or technologies generated in the work, or the application of information presented in the manuscript, pose a threat to:

| No Yes | | | | | | |
|---|--|--|--|--|--|--|
| Public health | | | | | | |
| National security | security | | | | | |
| Crops and/or livest | | | | | | |
| Ecosystems | | | | | | |
| Any other significan | nt area | | | | | |
| Experiments of concer | n | | | | | |
| Does the work involve an | y of these experiments of concern: | | | | | |
| No Yes | | | | | | |
| -,- | to render a vaccine ineffective | | | | | |
| | to therapeutically useful antibiotics or antiviral agents | | | | | |
| | nce of a pathogen or render a nonpathogen virulent | | | | | |
| | ibility of a pathogen | | | | | |
| Alter the host rang | | | | | | |
| | diagnostic/detection modalities nization of a biological agent or toxin | | | | | |
| | illy harmful combination of experiments and agents | | | | | |
| Z / my other potential | ing national combination of experiments and agents | | | | | |
| Plants | | | | | | |
| Seed stocks | | | | | | |
| Novel plant genotypes | | | | | | |
| Authentication | | | | | | |
| Additerrication | | | | | | |
| ChIP-seq | | | | | | |
| Data deposition | | | | | | |
| Confirm that both raw | v and final processed data have been deposited in a public database such as GEO. | | | | | |
| Confirm that you have | e deposited or provided access to graph files (e.g. BED files) for the called peaks. | | | | | |
| Data access links May remain private before public | cation. | | | | | |
| Files in database submiss | ion | | | | | |
| Genome browser session (e.g. <u>UCSC</u>) | | | | | | |
| Methodology | | | | | | |
| Replicates | | | | | | |
| Sequencing depth | | | | | | |
| Antibodies | | | | | | |
| Peak calling parameters | | | | | | |
| Data quality | | | | | | |
| Software | | | | | | |
| JUILWAIE | | | | | | |

| low Cytometry | |
|-------------------------------------|--|
| lots | |
| Confirm that: | |
| The axis labels state the marker | and fluorochrome used (e.g. CD4-FITC). |
| The axis scales are clearly visible | . Include numbers along axes only for bottom left plot of group (a 'group' is an analysis of identical markers). |
| All plots are contour plots with c | |
| A numerical value for number of | cells or percentage (with statistics) is provided. |
| /lethodology | |
| Sample preparation | |
| Instrument | |
| Software | |
| Cell population abundance | |
| Gating strategy | |
| Tick this box to confirm that a fig | gure exemplifying the gating strategy is provided in the Supplementary Information. |
| | |
| Magnetic resonance ima | ging |
| xperimental design | |
| Design type | |
| Design specifications | |
| Behavioral performance measures | |
| | |
| Imaging type(s) | |
| Field strength | |
| Sequence & imaging parameters | |
| Area of acquisition | |
| Diffusion MRI Used | ☐ Not used |
| reprocessing | |
| Preprocessing software | |
| Normalization | |
| Normalization template | |
| Noise and artifact removal | |
| Volume censoring | |
| Volume censoring | |
| tatistical modeling & inference | 2 |

Effect(s) tested

ROI-based

Both

| Harrie Politiono | |
|------------------|----------|
| | <u> </u> |
| | 5 |
| | |

| ₹ | د | |
|---|---|--|
| Ξ | | |
| | | |
| | | |
| | | |
| | | |
| | | |
| | | |
| Ċ | | |
| | ^ | |
| | | |
| | | |
| | | |

| Statistic type for inference | |
|-----------------------------------|---------------|
| (See Eklund et al. 2016) | |
| Correction | |
| Models & analysis | |
| n/a Involved in the study | |
| Functional and/or effective conne | ectivity |
| Graph analysis | |
| Multivariate modeling and predic | tive analysis |